Imaging of Plasmonic Heating in a Living Organism

Jon S. Donner,[†,§] Sebastian A. Thompson,[†,§] César Alonso-Ortega,[†] Jordi Morales,[†] Laura G. Rico,[†] Susana I. C. O Santos,[†] and Romain Quidant[†,‡,*]

[†]ICFO-Institut de Ciencies Fotoniques, Mediterranean Technology Park, 08860 Castelldefels, Barcelona, Spain and [‡]ICREA—Institució Catalana de Recerca i Estudis Avançats, 08010 Barcelona, Spain. [§]These authors contributed equally.

ABSTRACT Controlling and monitoring temperature at the single cell level has become pivotal in biology and medicine. Indeed, temperature influences many intracellular processes and is also involved as an activator in novel therapies. Aiming to assist such developments, several approaches have recently been proposed to probe cell temperature *in vitro*. None of them have so far been extended to a living organism. Here we present the first *in vivo* intracellular temperature imaging. Our technique relies on measuring the fluorescence polarization anisotropy of green fluorescent protein (GFP) on a set of GFP expressing neurons in *Caenorhabditis elegans* (*C. elegans*). We demonstrate fast and noninvasive monitoring of subdegree temperature changes on a single neuron induced by local photoheating of gold nanoparticles. This simple and biocompatible technique is envisioned to benefit several fields including hyperthermia treatment, selective drug delivery, thermal regulation of gene expression and neuron laser ablation.

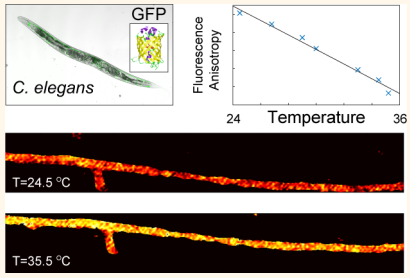

KEYWORDS: thermal imaging · intracellular temperature · *C. elegans* · plasmon heating · fluorescence imaging

Heat is of fundamental importance in all cellular processes, mechanics and bioreactions. The intracellular temperature changes, which follow the absorption or release of heat, can be divided into two groups: either the cell's activity induces a temperature change or the intracellular temperature changes because external heat is applied to obtain a desired cellular response. In both cases, obtaining an intracellular temperature map could reveal relevant information, especially if this could be done in the natural environment of the cell. Fields which would greatly benefit from this information include hyperthermia therapy,[1] photothermal therapy,[2,3] selective drug delivery using thermosensitive liposoms[4,5] or nanoparticles,[6] and gene regulation driven by heat shock protein promoters.[7] In the field of hyperthermia therapy, the temperature of tumor-loaded tissue is raised either to cause cell death or to increase the efficiency of conventional treatment such as radiotherapy or chemotherapy. These therapies involve nontrivial heating processes. Not only must the procedure adequately damage malignant tissue, but also the surrounding normal tissue should be unharmed. This becomes quite challenging, as the thermal characteristics of the tissue change during the ablation process. Furthermore, when heating with the aid of artificial photothermal agents, the temperature increase strongly depends on the density of these agents, which is usually hard to control and leads to inhomogeneous heating distributions. Therefore, real-time temperature mapping is necessary to serve as an input to a feedback loop of the heating process. Current methods to measure temperature in tissue include magnetic resonance imaging[8] (MRI) and thermistors;[1] however, these methods can suffer from disadvantages, such as complex machinery for MRI or an invasive measurement for thermistors, and none of them have yet achieved thermal imaging in a live organism on a subcellular resolution. To achieve the highest level of specificity in hyperthermia techniques, the spatial resolution should be at the cellular scale. However, obtaining the temperature over such a small spatial resolution has proven to be a difficult task. Since 1995, when the first cellular temperature probe was reported,[9] a plethora of new methods have been developed[10,11] and over 20 thermal probes presented. Some examples include quantum dots,[12,13] nanoparticles,[14] submicrometer thermocouple,[15] nanogels,[16] copolymers[17] and NV centers.[18] Also, recently,

* Address correspondence to romain.quidant@icfo.es.

Received for review June 7, 2013 and accepted September 18, 2013.

Published online September 18, 2013
10.1021/nn403659n

cellular thermal imaging was achieved by using photoacoustic microscopy.[19,20] All these methods have only been demonstrated *in vitro* (by *in vitro* the authors refer to experiments performed on cultured cells whereas *in vivo* referees to experiments using intact organisms). Translation from basic *in vitro* research to an *in vivo* model can be crucial and is considered a scientific milestone in many biomedical fields. However, *in vitro* research cannot always be translated to *in vivo* models. Moreover, in many cases clear discrepancies have been shown between *in vitro* and *in vivo* studies.[21] Indeed, none of the reported thermal probes have so far been successfully applied to an *in vivo* model mostly because all of these methods rely on the introduction of foreign thermosensitive or absorption contrast agents into cells either by endocytosis or microinjection techniques. Furthermore, the concentration of these compounds within the cell must be optimized, a very challenging task when performed in an *in vivo* specimen. In addition, selective delivery of the thermal compounds to specific target cells in a live organism can be difficult, even impractical, whereas in the *in vitro* case, this concern does not exist as they usually involve a single cell type. Moreover, it will be hard to predetermine whether these compounds will be toxic or affect the basal conditions of the studied organism. Finally, it is not clear whether the reported probes will remain active once introduced into a live organism.

In this study we believe to be the first to report intracellular temperature mapping in an *in vivo* model. This method, which overcomes the previously mentioned difficulties, is based on measuring the fluorescence polarization anisotropy (FPA) of green fluorescent protein (GFP) allowing a fast, accurate, and noninvasive measurement in a live organism on a subcellular spatial scale. In a previous communication, we reported the ability to map temperature in an *in vitro* environment.[22] Because of the GFP's biocompatibility, and its ubiquitous use in *in vivo* scientific models, we were able to cross the chasm separating *in vitro* from *in vivo* measurements. The method is demonstrated on a permanently transfected *Caenorhabditis elegans* (*C. elegans*) strain expressing the GFP marker in the GABAergic neurons. The *C. elegans* is a well-accepted *in vivo* model[23] that supports many advantages. The fact that genetically modified cells express the thermal probe, GFP, has several advantages: first, it permits an established "insertion" of a probe which does not affect the cellular mechanisms and processes; also, GFP can be selectively expressed only in the target cells of interest. The concentration of expressed GFP in permanent transfected species does not affect our measurements as FPA is a ratio of intensities; this also renders the FPA measurement nonsensitive to fluctuations of the excitation laser intensity, photobleaching, and probe migration. The technique enables us to monitor small changes in the distribution of temperature in a single neuron of the *C. elegans*. We present two different experimental configurations: first, when heat is delivered from outside the worm, and second, when heat is generated inside the *C. elegans* by local photoheating of ingested gold nanoparticles.

RESULTS

Anisotropy as a Temperature Reporter in *C. elegans* Neurons. The underlying physics relating temperature and molecular FPA is well established and has been previously reported and explained.[22,24,25] Briefly, the FPA is directly related to rotational diffusion induced by molecular Brownian dynamics, hence, the relation to temperature. Specifically, the rotational motion of the molecules is related to temperature *via* the Debye–Stokes–Einstein equation:[26]

$$\tau_R = \frac{V\eta(T)}{k_B T} \quad (1)$$

where τ_R is the rotational lifetime, T is the temperature, $\eta(T)$ is the viscosity, V is the hydrodynamic volume of the fluorophore, and k_B is the Boltzmann constant . The molecular rotation caused by Brownian dynamics is related to the FPA, r, according to Perrin's equation:

$$\frac{1}{r} = \frac{1}{r_0}\left(1 + \frac{\tau_F}{\tau_R}\right) \quad (2)$$

where τ_F is the fluorescence lifetime and r_0 is the limiting polarization anisotropy in the absence of any molecular motion ($\leq$0.4). Note that the maximum temperature sensitivity is reached when τ_R is on the order of τ_F. The fluorescence lifetime is given by the GFP and has been reported to be on the order of τ_F = 2.5 ns. The rotational lifetime, at a given temperature, depends both on the intracellular microviscosity and the protein's hydrodynamic volume. In the example presented in this report, we used GFP tagged to the enzyme glutamic acid decarboxylase (GAD), which is expressed only in the GABAergic neurons of the *C. elegans*. The main function of GAD involves a single step synthesis of the neurotransmetter GABA . The GAD–GFP complex is known to be located in the cell bodies, axon branches and synapses regions of these neurons and is believed to remain unbound[27] and thus free to rotate. An experimental curve relating FPA of the GAD–GFP to temperature in an *in vivo* model was performed to obtain the real relationship between the anisotropy of GAD–GFP complex and temperature. This was done by placing the GFP transfected worms on a coverslip connected to an external electrical heater. The temperature was varied in the range 24–35 °C, and kept well below temperatures that would cause biological damage. The temperature was varied slowly so that the temperature of the neurons was assumed to be equal to that of the heater. At different temperatures, a confocal scan was performed giving an FPA map, as can be seen in Figure 1e–g.

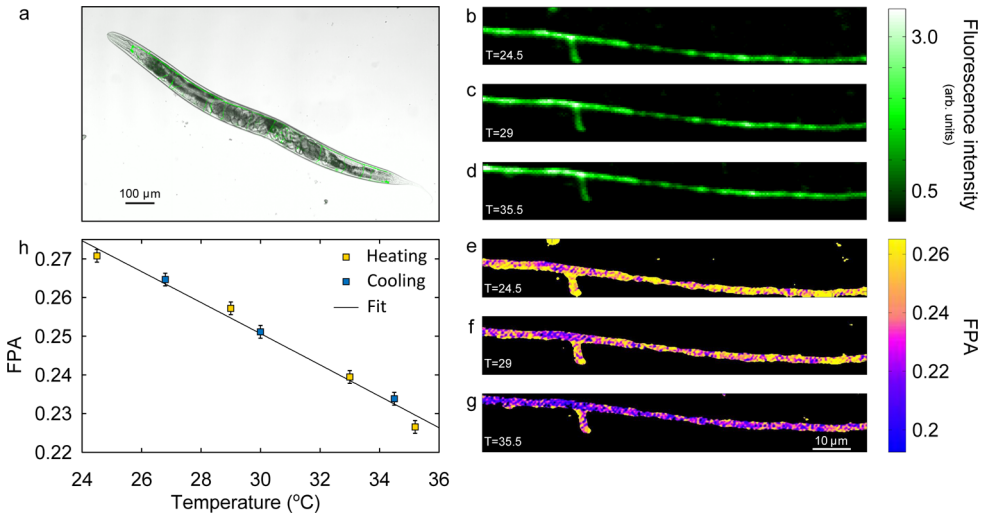

Figure 1. FPA *vs* temperature calibration measurements in *C. elegans*. (a) Bright-field image of the *C. elegans* overlapped with the GFP fluorescence intensity coming from the GABAergic neurons in green. (b–d) GFP fluorescence intensity from the same set of transfected neurons at three different temperatures. Over this range of temperatures, the intensity variation is very small. (e–g) FPA of the same neurons at these same three temperatures. (h) Curve showing the relationship between the average FPA and the temperature while heating and cooling the system in yellow and blue, respectively.

These images were taken when heating the system and also when cooling the system down to verify reversibility. The scan is performed with a collection time of 2 ms per pixel, and the entire image takes about 1 min to record. Indeed, the FPA decreases as the temperature rises, as expected. These results are summarized in Figure 1h, which is an *in vivo* calibration curve. Each point is calculated by taking a spatial average of the measured FPA map in the *C. elegans* of the corresponding temperature. This curve presents an impressive sensitivity, given by the variation of FPA over this temperature range of about 0.004 $°C^{-1}$ (large compared to a value of a nontagged GFP in water which is about 0.001 $°C^{-1}$ [22]). From this high sensitivity we can deduce that the fluorescence lifetime is on the same order of the rotational lifetime. It is worth noting that over this relatively small temperature range (24–35 °C) the intensity of the GFP fluorescence does not change notably as can be seen in Figure 1b–d.

We observe that the FPA maps are uniform, although the intensity maps are not (see Figure S1 in Supporting Information). Because FPA is a ratio of intensities, it is not influenced by variations in the fluorescence intensity. The uniform FPA also implies a homogeneous intracellular viscosity, which is consistent with the observations in Kalwarczyk *et al.*[28] whereby it was shown that a probe the size GFP (smaller than tens of nanometers) experiences a nanoviscosity which is not affected by the larger organelles or macromolecules inside the cell. Finally, the uniform FPA map (uniform within experimental noise limits) also implies that the GAD–GFP complex does not bind to specific cellular structures. To estimate the temperature sensitivity, data was acquired from one location during 20 s, at a rate of 0.3s per data point. The standard deviation of this data set was taken to be the measurement error (and was the size of the error bars in Figure 1h); this calculation gave a value corresponding to 0.8 °C, which is comparable with reported thermal sensitivity of luminescent nanothermometers of 0.18–4 °C[10,11] (note however that these sensitivities were not measured in a single standardized way). The temperature during the measurement was constant, and so the standard deviation gives an indication of the temperature error introduced by the measurement. The reliability of this method at different pH levels has been previously shown[22] by performing FPA temperature calibration curves of GFP in a PBS solution at pH levels between 6.0 and 7.4, which span most of the intracellular pH levels. These measurements were performed between room temperature and 60 °C both when heating the system and when cooling it down, which shows reversibility over a wide range of temperatures.

Intracellular Temperature Mapping Induced by External Photoheating. Once the calibration curve was obtained, we performed an experiment in which we map the temperature change inside the *C. elegans* resulting from external photoheating. Heating was induced by illuminating GNRs dispersed in the medium surrounding the worm. For an incident wavelength matching their plasmon resonance, the GNRs efficiently convert the laser power to heat providing quick and local heating of the specimen. It should, however, be stated that any other generic heating method could be used. In this experiment, the GNRs were placed and illuminated outside the *C. elegans*, emulating configurations where external heat is applied to obtain a desired cell activity, such as the use of thermo polymers for drug delivery. In this context, temperature mapping will help to understand the quantity, distribution, and time

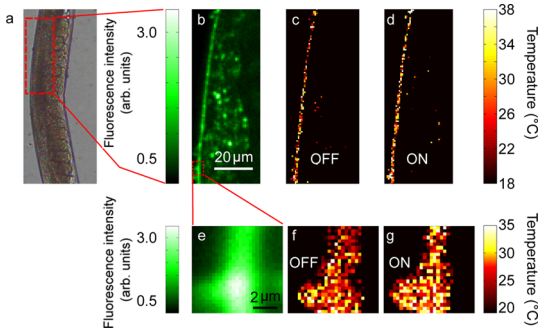

Figure 2. Intracellular temperature measurements in *C. elegans* induced by external heating: (a) bright field image of *C. elegans*; (b) fluorescence intensity of GFP transfected neurons in the *C. elegans*; (c) temperature image of the neurons when the laser is off; (d) temperature image of the neurons when the laser is on and focused onto GNRs which are located outside the worm. The laser has a power of P = 50 mW (63 kW/cm^2) and is focused 50 μm to the left of the worm (specifically, 50 μm to the left of the bottom left corner of the red square in panel a). (e–g) Repeating the previous experiment while zooming in and imaging a smaller area.

constants of the delivered heat at the target cell. Figure 2c,d illustrates the temperature mapping of the *C. elegans* neurons without and with application of heat to the system. A small change in the temperature can be observed over the entire image. Figure 2e–g shows a higher resolution scan on a smaller region in which the temperature change is mapped on a subcellular scale. An average raise of temperature of 2 °C is measured. As the fluorescence intensity of the GFP is much higher than the intrinsic auto fluorescence, a digital intensity threshold is applied to obtain FPA information only from the GAD–GFP and not the surrounding intrinsic auto fluorescence of the *C. elegans*. It is worth mentioning that, because we are measuring neurons in a live organism, they have a 3D structure (as opposed to a 2D, flat geometry of the cells in an *in vitro* model); however, due to the *z*-plane sectioning that is achieved by a confocal system, signal from out of the imaging plane is automatically filtered out.

Intracellular Temperature Mapping Induced by Internal Photoheating. As another example of use of our method, we performed an experiment in which heat was locally generated from within the *C. elegans* and the resulting temperature changes were mapped in real time. This is an important practical example because it concurs with the approach used in fields of photothermal cancer therapy. The *C. elegans* were fed overnight with the GNRs (see Materials and Methods), which accumulated in the worms' digestive tract. The worms were anesthetized and immediately used for experimentation; thus, the concentration of GNRs inside the organism remains constant during the duration of the experiment. No effect on the dynamics of the *C. elegans* has been observed due to the GNRs. Figure 3a shows an example of presence and location of the GNRs which were identified using two-photon fluorescence

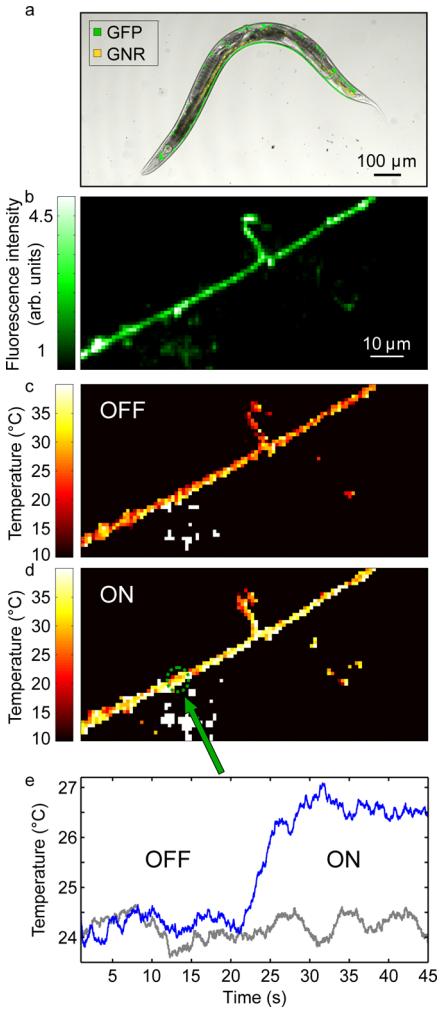

Figure 3. Intracellular temperature measurements induced by internal heating. The experiment is performed on a worm with GFP transfected neurons and GNRs inside its body. (a) Bright field image of *C. elegans* overlapped with the GFP fluorescence intensity coming from the GABAergic neurons in green, and the two-photon fluorescence signal coming from GNRs in yellow. The GNRs are concentrated in the worm's digestive tract. (b) Fluorescence intensity of GFP transfected neurons in the *C. elegans*. (c) Temperature image of the neurons when the laser is off. (d) Temperature image of the neurons when the laser is on. The laser is focused onto GNRs inside the *C. elegans* and is located about 50 μm away from the center of the neurons in the perpendicular direction. The power is set to P = 100 mW (127 kW/cm^2). The heating is generated *via* photothermal conversion of GNRs, which are inside the worm (GNRs are located as in panel a). (e) Temperature measured at one point as a function of time. The point is marked with the green arrow. The laser was turned on at t = 20 s, and the subsequent change of temperature was measured and presented in the blue curve (the laser was focused onto GNRs inside the worm and was set to a power of P = 50 mW (63 kW/cm^2)). A control experiment performed on a worm with no GNRs and illuminated under similar conditions is presented in the gray curve. The heating laser was turned off after almost 2 min and the temperature trace is presented in Figure S3 of Supporting Information.

nonlinear microscopy. Figure 3b–d shows the temperature change of the neurons when switching on the NIR laser which heated the GNRs. The first notable

feature is that the temperature rises uniformly over the scanned region (about 100 μm). As expected, heating from inside the worm is more efficient than heating from the outside. As an important final experiment, a real time temperature measurement was measured in a fixed position while the intensity of the NIR laser switched between off and on. Time-evolution of the temperature is presented in Figure 3e, in which the data was collected on a time scale of 20 ms per/data point. Shining the GNRs with a 50 mW (which gives a power density of 63 kW/cm^2 at focal plane) laser induces a change in temperature of almost 3 °C. This experiment was reproduced for different powers, which gave a linear dependence of the temperature on the incoming laser power, as expected (see Figure S2 in Supporting Information). Similar power densities shone on GNRs, which generated a comparable temperature rise, have been previously reported in the literature[29] (100 kW/cm^2 which generated about a 2 °C temperature raise). Because of a different system and specifically a different GNR concentration and distribution, the heating is not expected to give the exact same results. The temperature rises until a point where a thermal equilibrium is attained and the temperature reaches a plateau, a typical behavior of a heated open system.[30] The rise time of the temperature is in the seconds range. This is a longer than expected time when heating an area of micrometric dimensions.[31] We attribute this discrepancy to the fact that heating of GNRs occurs out of the focal plane of the 800 nm laser in the entire digestive system of the *C. elegans*, increasing the volume of the heated region and thus the thermalization time. When the heating source is turned off, the temperature returns to a level near the original baseline (see Figure S3 in Supporting Information). Another experiment was performed on a different worm that was not incubated with GNRs. The worm was illuminated under similar conditions (similar power and distance from measurement point). The resulting temperature is presented in the gray curve in Figure 3e. As expected, the temperature does not rise when the laser is on, which confirms that the photothermal conversion is induced by the GNRs and not by the *C. elegans* tissue. Ultimately, such dynamic temperature monitoring could be useful, for example, to track the temperature change during neuron synapses or reticulum endoplasmic calcium release in mammalian cells.

DISCUSSION AND CONCLUSIONS

In this study, we demonstrated the first *in vivo* intracellular temperature mapping technique in a live model organism. This was achieved by monitoring the FPA of GAD−GFP protein complex, which was permanently expressed in the GABAergic neurons of the *C. elegans* soil worm. However, the applicability of the method is not restricted to this specific protein complex or with this living organism. The implementation of the method on other organisms will be greatly facilitated by the extended usage of GFP transfected models. When using this technique with GFP tagged to other proteins, one should expect a different accuracy of the temperature measurement. The different protein complexes will have different rotational lifetimes than that of GAD−GFP, which then will change the calibration curve relating FPA to temperature. In practice, the relation between the FPA and the temperature of the new protein complex must be remeasured (the equivalent of Figure 1h). To be able to accurately measure local temperature, the FPA−temperature calibration curve must fulfill two requirements: first, the FPA map must be uniform (to a level possible given the measurement noise), and the curve must be reproducible (*i.e.*, when lowering the temperature one must obtain the same FPA value). The uniformity implies that the used probe experiences a uniform viscosity in the cell, and does not bind to specific intracellular structures. The reproducibility implies that no changes in protein structure have occurred and that if any protein binding occurs, this is factored into the measured FPA. In the case that part of the proteins bind to cellular structures (even if the binding depends on temperature), the FPA reading will be modified, and the sensitivity of the measurement will be reduced, but the FPA calibration curve will still give accurate results. Thereafter, intracellular temperature can be directly monitored by measuring FPA; this can be done either to obtain temperature imaging (similar to Figure 3c,d) or real time temperature measurements (as in Figure 3e). We have seen that the GAD−GFP complex delivers superior accuracy compared to a nontagged GFP; we do expect there to be further optimization to this accuracy by using proteins of other size and structure to GFP.

We also believe that a pertinent line of investigation is to apply the method to perform temperature measurements in different tissues, where the intracellular temperature of cells is measured together with the extracellular matrix. Also, to better improve tissue penetration, different fluorescent proteins such as red fluorescent protein and its derivatives can be used where the fluorescence spectral window matches that of tissue transparency window.

When applying this method to nontransparent tissues, the randomness of the tissue structure and the multiple scattering events will result in depolarization of the propagating light. In strongly scattering tissue, the depolarization length, defined as the length where the ratio $I_{\parallel}/I_{\perp}$ decreases by 2, where $I_{\parallel}$ and $I_{\perp}$ are the intensities of the fluorescence polarized parallel and perpendicular to the incident polarization, depends on the tissue and wavelength. Characteristic lengths are 0.2 until about 4 mm for white matter of brain and whole blood with a low level of hematocrit, respectively.[32]

For transparent tissues such as eye tissues, cellular monolayers, mucous membrane, and superficial skin layers, the polarization of transmitted light remains measurable for longer thicknesses.

MATERIALS AND METHODS

Used Specimen and Sample Preparation. The experiments presented in our article have been performed with the model organism *Caenorhabditis elegans*. Specifically, the worm strain with the juls76 [unc-25::GFP] II genotype that expresses the green fluorescence protein (GFP) attached to the GAD protein in the 26 GABAergic neurons' cytosol.

Two cultures of the same strain were routinely grown in the laboratory in liquid S media, at 20 °C and fed on the nonpathogenic bacteria *Escherichia coli* strain OP50. One of the cultures was supplemented with gold nanorods (GNRs) at final concentration of 0.2 ng/L. Gold nanorods were synthesized and purified, and the ligands were exchanged as described elsewhere.[22] For the sample preparation, adult worms were anesthetized with 4 μL of sodium azide, 35 mM (NaN_3, Scharlau, Spain) and mounted on a 1% agar pad (Agarose low EEO, Scharlau, Spain) between two glass coverslips (Menzel Gläser, Germany). These agar pads prevent nematodes from dehydration and from being crushed between the two coverslips. Finally, the samples were sealed with melted paraffin for sample stability.

Three different experiments were run: (1) worms grown in the absence of GNRs were mounted (as explained above) and placed over a controlled heating-source in order to measure the calibration curve relating FPA and temperature. (2) Worms grown in the absence of GNRs were mounted with the addition of 3 μL of 1 ng/l solution of GNRs between the agar pad and the coverslips. These were subjected to temperature changes to monitor temperature during external heating. (3) Worms cultured and fed with GNRs were mounted and subjected to temperature changes by heating the GNRs inside the worm's gut in order to monitor the temperature during internal heating.

Fluorescence Microscopy and Anisotropy Imaging. A detailed description of the fluorescence and anisotropy microscopy was presented in ref 25. The GFP molecules were excited with a blue diode laser λ = 473 nm. The beam was focused with a 10× objective (UPlanFLN, N.A. 0.3, Olympus) and scanned with a scanning mirror (FSM-300, Newport) in a 4f system. The scans are performed with a collection time of 2−20 ms per pixel, and the images take between 0.5 and 2 min to record. In all experiments, the blue laser intensity was below 1 μW before the objective. The GFP fluorescence was sent through a polarization beam splitter and recorded simultaneously on two APDs (MPD-PDM series). The blue and red lasers were filtered out of the detection optical path using optical filters (Semrock: BLP01-488R-25, BLP01-473R-25, SP01-785RU-25). The anisotropy was calculated using the following formula:

$$r = \frac{I_{\parallel} - I_{\perp}}{I_{\parallel} + 2I_{\perp}}$$

where $I_{\parallel}$ and $I_{\perp}$ are the intensities of the fluorescence polarized parallel and perpendicular to the incident polarization. The surrounding intrinsic autofluorescence of the *C. elegans* was separated from the fluorescent signal of the GFP by using an intensity threshold (as the GFP fluorescence is much stronger than that of the auto fluorescence of the surrounding tissue). A digital correction of APD fine alignment was done by measuring the cross correlation of the two APD images.

***C. elegans* Temperature Mapping When Heating with GNRs.** Heating of gold nanorods was performed using a CW IR laser beam from a Ti:sapphire (mira 900, Coherent), and its wavelength set to λ = 800 nm (corresponding to the longitudinal GNR plasmon resonance), focused through a 50 mm lens. Temperature mapping as in Figure 2 was done by focusing the heating laser to a spot 50 μm away from the *C. elegans* body, which was placed at room temperature. The FPA of the GFP labeled neurons was imaged, by scanning the blue laser beam, with and without heating. The temperature was then calculated from the FPA using a calibration curve, like that presented in Figure 1h.

In Figure 3, the red heating laser was pointed to an area of the worms' digestive tract with GNRs inside the worm (radius of laser at GNRs was ≅5 μm). The GNRs were located with two-photon microscopy (as in Figure 3a). The resulting FPA was measured and converted to a temperature map. Temperature measurement as function of time, as presented in Figure 3e, was performed by setting the blue probe laser beam (λ = 473 nm) to a fixed position and modifying the power of the red heating laser (in this case the IR laser was heating GNRs inside the worm), the resulting FPA recorded, from which the temperature was calculated. A smoothing function was applied to this measurement (Figure 3e), where each point was taken to be the average over 0.6 s of acquired data.

Conflict of Interest: The authors declare no competing financial interest.

Acknowledgment. The authors wish to thank Dr. G. Baffou form Institut Fresnel (Marseille, France) for fruitful discussions. The authors also thank Dr. Joe Culotti, from the Samuel Lunenfeld Research Institute (Toronto, Canada), who provided us with the GFP labeled worm strain. This research has been partially supported by Fundació Privada Cellex and has been conducted at ICFO's "Super-Resolution Light Microscopy and Nanoscopy Facility" (SLN@ICFO).

Supporting Information Available: High resolution fluorescence imaging of transfected neurons of *C. elegans*; linear dependence of temperature on incoming laser power; reversibility of temperature measurement. This material is available free of charge *via* the Internet at http://pubs.acs.org.

REFERENCES AND NOTES

1. Wust, P.; Hildebrandt, B.; Sreenivasa, G.; Rau, B.; Gellermann, J.; Riess, H.; Felix, R.; Schlag, P. M. Hyperthermia in Combined Treatment of Cancer. *Lancet Oncol.* **2002**, *3*, 487–497.
2. West, J. L. Nanoshell-Mediated Near-infrared Thermal Therapy of Tumors Under Magnetic Resonance Guidance. *Proc. Natl. Acad. Sci. U.S.A.* **2003**, *100*, 13549–13554.
3. Bardhan, R.; Lal, S.; Joshi, A.; Halas, N. J. Theranostic Nanoshells: From Probe Design to Imaging and Treatment of Cancer. *Acc. Chem. Res.* **2011**, *44*, 936–946.
4. Koning, G.; Eggermont, A. M.; Lindner, L.; Hagen, T. M. Hyperthermia and Thermosensitive Liposomes for Improved Delivery of Chemotherapeutic Drugs to Solid Tumors. *Pharm. Res.* **2010**, *27*, 1750–1754.
5. Dicheva, B. M.; ten Hagen, T. L. M.; Li, L.; Schipper, D.; Seynhaeve, A. L. B.; van Rhoon, G. C.; Eggermont, A. M. M.; Lindner, L. H.; Koning, G. A. Cationic Thermosensitive Liposomes: A Novel Dual Targeted Heat-Triggered Drug Delivery Approach for Endothelial and Tumor Cells. *Nano lett.* **2013**, *13*, 2324–2331.
6. Luo, Y.-L.; Shiao, Y.-S.; Huang, Y.-F. Release of Photoactivatable Drugs from Plasmonic Nanoparticles for Targeted Cancer Therapy. *ACS Nano* **2011**, *5*, 7796–7804.
7. Kamei, Y.; Suzuki, M.; Watanabe, K.; Fujimori, K.; Kawasaki, T.; Deguchi, T.; Yoneda, Y.; Todo, T.; Takagi, S.; Funatsu, T.; *et al.* Infrared Laser-Mediated Gene Induction in Targeted Single Cells *in Vivo*. *Nat. Methods* **2009**, *6*, 79–81.
8. Galiana, G.; Branca, R. T.; Jenista, E. R.; Warren, W. S. Accurate Temperature Imaging Based on Intermolecular Coherences in Magnetic Resonance. *Science* **2008**, *322*, 421–424.
9. Chapman, C. F.; Liu, Y.; Sonek, G. J.; Tromberg, B. J. The Use of Exogenous Fluorescent Probes for Temperature Measurements in Single Living Cells. *Photochem. Photobiol.* **1995**, *62*, 416–425.
10. Jaque, D.; Vetrone, F. Luminescence Nanothermometry. *Nanoscale* **2012**, *4*, 4301–4326.

11. Brites, C. D. S.; Lima, P. P.; Silva, N. J. O.; Millan, A.; Amaral, V. S.; Palacio, F.; Carlos, L. D. Thermometry at the Nanoscale. *Nanoscale* **2012**, *4*, 4799–4829.
12. Maestro, L. M.; Rodríguez, E. M.; Rodríguez, F. S.; Cruz, M. C. I.; Juarranz, A.; Naccache, R.; Vetrone, F.; Jaque, D.; Capobianco, J. A; Solé, J. G. CdSe Quantum Dots for Two-Photon Fluorescence Thermal Imaging. *Nano lett.* **2010**, 5109–5115.
13. Yang, J.; Yang, H.; Lin, L. Quantum Dot Nano Thermometers Reveal Heterogeneous Local Thermogenesis in Living Cells. *ACS Nano* **2011**, *5*, 5067–5071.
14. Vetrone, F.; Naccache, R.; Zamarrón, A.; Juarranz de la Fuente, A.; Sanz-Rodríguez, F.; Martinez Maestro, L.; Martín Rodriguez, E.; Jaque, D.; García Solé, J.; Capobianco, J. A. Temperature Sensing Using Fluorescent Nanothermometers. *ACS Nano* **2010**, *4*, 3254–3258.
15. Wang, C.; Xu, R.; Tian, W.; Jiang, X.; Cui, Z.; Wang, M.; Sun, H.; Fang, K.; Gu, N. Determining Intracellular Temperature at Single-Cell Level by a Novel Thermocouple Method. *Cell Res.* **2011**, *21*, 1517–1519.
16. Gota, C.; Okabe, K.; Funatsu, T.; Harada, Y.; Uchiyama, S. Hydrophilic Fluorescent Nanogel Thermometer for Intracellular Thermometry. *J. Am. Chem. Soc.* **2009**, *131*, 2766–2767.
17. Okabe, K.; Inada, N.; Gota, C.; Harada, Y.; Funatsu, T.; Uchiyama, S. Intracellular Temperature Mapping with a Fluorescent Polymeric Thermometer and Fluorescence Lifetime Imaging Microscopy. *Nat. Commun.* **2012**, *3*, 1–9.
18. Kucsko, G.; Maurer, P. C.; Yao, N. Y.; Kubo, M.; Noh, H. J.; Lo, P. K.; Park, H.; Lukin, M. D. Nanometre-Scale Thermometry in a Living Cell. *Nature* **2013**, *500*, 54–58.
19. Gao, L.; Wang, L.; Li, C.; Liu, Y.; Ke, H.; Zhang, C.; Wang, L. V. Single-Cell Photoacoustic Thermometry. *J. Biomed. Opt.* **2013**, *18*, 026003.
20. Gao, L.; Zhang, C.; Li, C.; Wang, L. V. Intracellular Temperature Mapping with Fluorescence-Assisted Photoacoustic-Thermometry. *Appl. Phys. Lett.* **2013**, *102*, 193705–193710.
21. Schurgers, E.; Kelchtermans, H.; Mitera, T.; Geboes, L.; Matthys, P. Discrepancy Between the *in Vitro* and *in Vivo* Effects of Murine Mesenchymal Stem Cells on T-Cell Proliferation and Collagen-Induced Arthritis. *Arthritis Res. Ther.* **2010**, *12*, 1–11.
22. Donner, J. S.; Thompson, S. A.; Kreuzer, M. P.; Baffou, G.; Quidant, R. Mapping Intracellular Temperature Using Green Fluorescent Protein. *Nano Lett.* **2012**, *12*, 2107–2111.
23. Saito, R. M.; van den Heuvel, S. Malignant Worms: What Cancer Research Can Learn from *C. elegans*. *Cancer Invest.* **2002**, *20*, 264–275.
24. Zondervan, R.; Kulzer, F.; van der Meer, H.; Disselhorst, J. A. J. M.; Orrit, M. Laser-Driven Microsecond Temperature Cycles Analyzed by Fluorescence Polarization Microscopy. *Biophys. J.* **2006**, *90*, 2958–2969.
25. Baffou, G.; Kreuzer, M. P.; Kulzer, F.; Quidant, R. Temperature Mapping Near Plasmonic Nanostructures Using Fluorescence Polarization Anisotropy. *Opt. Express* **2009**, *17*, 3291–3298.
26. Valeur, B. *Molecular Fluorescence: Principles and Applications*; Wiley-VCH: New York, 2001.
27. Jin, Y.; Jorgensen, E.; Hartwieg, E.; Horvitz, H. R. The Caenorhabditis Elegans Gene unc-25 Encodes Glutamic Acid Decarboxylase and Is Required for Synaptic Transmission but Not Synaptic Development. *J. Neurosci.* **1999**, *19*, 539–548.
28. Kalwarczyk, T.; Zie, N.; Hozyst, R.; Wyszy, C. S. Comparative Analysis of Viscosity of Complex Liquids and Cytoplasm. *Nano Lett.* **2011**, 2157–2163.
29. Maestro, L. M.; Haro-González, P.; Iglesias-de la Cruz, M. C.; Sanz-Rodríguez, F.; Juarranz, Á.; Solé, J. G.; Jaque, D. Fluorescent Nanothermometers Provide Controlled Plasmonic-Mediated Intracellular Hyperthermia. *Nanomedicine* **2012**, *8*, 379–388.
30. Richardson, H. H.; Carlson, M. T.; Tandler, P. J.; Hernandez, P.; Govorov, A. O. Experimental and Theoretical Studies of Light-to-Heat Conversion and Collective Heating Effects in Metal Nanoparticle Solutions. *Nano Lett.* **2009**, *9*, 1139–1146.
31. Donner, J. S.; Baffou, G.; McCloskey, D.; Quidant, R. Plasmon-Assisted Optofluidics. *ACS Nano* **2011**, *5*, 5457–5462.
32. Tuchin, V. V. *Tissue Optics: Light Scattering Methods and Instruments for Medical Diagnosis*, 2nd ed.; SPIE: Bellingham, WA, 2007.